Supplementary Material for

Simultaneous electric production and sizing of emulsion droplets in microfluidics

Sang Jun Lee, Ji Yoon Kang, Wonjoon Choi, and Rhokyun Kwak

1. Microchannel dimensions and electrical resistances

W [μm]	H [μm]	L [μm]	L/D_H
10	10	25	2.5
20	15	100	5.8
10	10	100	10
20	5	100	12.5

Table S1. Channel-neck dimensions of the fabricated devices for the buffer-less electric emulsification platform and the aspect ratios (length/hydraulic diameter).

Table S1 presents the channel-neck dimensions used for the experiments. D_H represents the hydraulic diameter of the channel neck, which can be calculated as $2WH/(W+H)$.

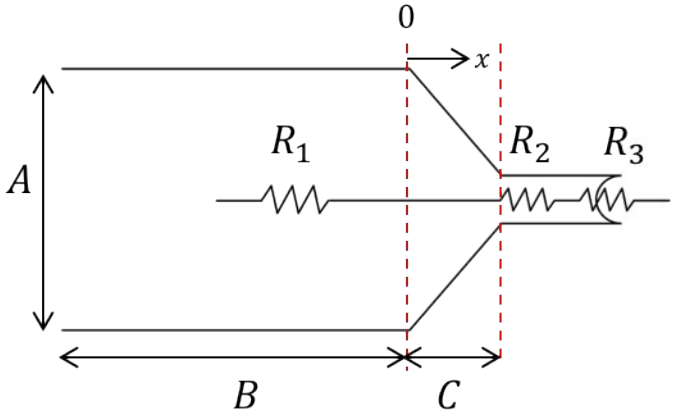

Figure S1. Electrical resistance model for the entire microchannel, consisting of a long microchannel (R_1), channel neck (R_2), and liquid/liquid interface (R_3).

R_1, R_2, and R_3 represent the electrical resistances of the long microchannel, channel neck, and liquid/liquid interface, respectively. R_3 is calculated at SI2. The entire channel has a height of H, and the channel neck has a width of W and a length of L. The entire long microchannel and

channel necks are first filled with the continuous phase, which has an electrical resistivity of ρ_c. Then, according to the geometric characteristics of the wide channel, R_1 can be calculated as

$$R_1 = \rho_c\left(\frac{B}{AH} + \int_0^C \frac{1}{H(3.62x + 5)}dx\right). \quad \text{(S1)}$$

The second term in Eq. (S1) inside the integral is used to compute the electrical resistance of the converging part of the wide channel (part *C* in Fig. S1). Because of the converging geometry of this narrowing part, the width varies with respect to x. The term in the denominator denotes this changing width considering the slope of the narrowing geometry. Likewise, R_2 can be calculated as

$$R_2 = \rho_c\frac{L}{WH}. \quad \text{(S2)}$$

The reservoirs for the continuous and dispersion phases are circular in shape, with a diameter of 2 mm. The electrical resistances of the reservoirs, R_{res}, can be derived as follows (where ρ_c and ρ_d represent the electrical resistivities of the continuous and dispersion phases, respectively):

$$R_{res} = \rho_c \times \frac{10^{-3}}{\pi \times 10^{-6}} + \rho_d \times \frac{10^{-3}}{\pi \times 10^{-6}}. \quad \text{(S3)}$$

As shown in the table summarizing R_1, R_2, R_3, and R_{res} in the next section, R_{res} for each channel was significantly lower than ($R_1 + R_2 + R_3$). Therefore, it is reasonable to ignore the effects of R_{res} for all the experiments.

The electric field dissipated at the continuous phase (R_1 and R_2) plays no role in the interface motion and the emulsification process. Therefore, the electric-field strength should be adjusted to reflect only the electric field applied across the interface (R_3) when calculating the electrical Weber number (We_e). The electric field across the interface, E_{in}, can be calculated as

$$E_{in} = \frac{(\frac{R_3}{R_1 + R_2 + R_3}) \cdot V}{l}, \quad \text{(S4)}$$

where V represents the applied voltage across the entire channel, and l represents the length that interface reaches inside the channel neck.

2. Electrical resistances of interface

(a) Current–voltage response

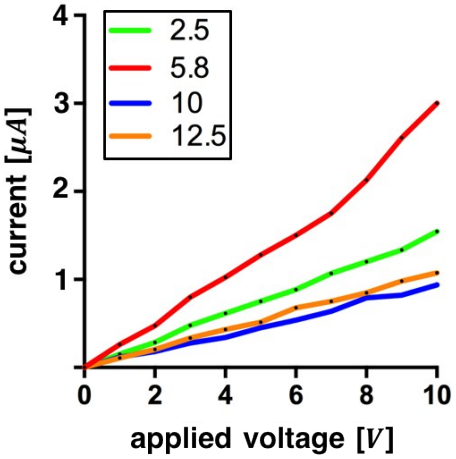

Figure S2. Current–voltage graph for each channel, with the applied voltage ranging from 0–10 V.

In the previous section, the theoretical electrical resistances of the channels were calculated as $R_1 + R_2$. These calculated values were compared with the actual electrical resistances of the channels, which were obtained by tracing the current values based on the applied external voltages, as shown in Fig. S2. The theoretical and experimental values exhibited discrepancies.

Fig. S2 indicates that the actual electrical resistances were 6.5, 4.1, 11.1, and 9.2 $M\Omega$ for channels with aspect ratios of 2.5, 5.8, 10, and 12.5, respectively. The difference between the actual resistance and the theoretical value, $R_1 + R_2$, was considered to be the electrical resistance of the interface, R_3, throughout the theoretical and experimental analyses, because no factor other than the existence of the interface could cause this difference. Because there were no

other solutes inside the liquid phases (such as particles or surfactants) that could pollute the electrode surface in a short time, we did not consider the effect of electrode fouling. Thus, we could produce monodisperse emulsions without significant changes in the normalized current peaks over 2 min, as shown in Fig. 2 of the manuscript (Supplementary Material Section 4). This indicates that no changes in the electrical properties of the electrode surface should be considered for that time duration. However, the production of debris during the emulsification may have nonnegligible influences on the electrode fouling and necessitate additional surface treatments.

The electrical resistances of the different parts of the microchannels are presented in Table S2. The high electrical resistance inside the channel-neck region created an electric field of O(10^3) V/m in the dripping and cone-jetting regimes (applied voltage of 30–90 V). This electric field increased the temperature inside the channel by approximately 5 ℃ for 20 s owing to the Joule heating effect[1]. Forciniti *et al.*[2] confirmed that this amount of temperature difference play no role in changing the interfacial tension between PEG-rich and Dextran-rich phase. Thus, we safely ignored the effect of the electric field-induced Joule heating in this study. In addition, the electric field of O(10^3) V/m results in the electroosmotic velocity ($v_{eof} = (\varepsilon\zeta/4\pi\mu)E$, ζ is zeta potential of PDMS wall) of O(10^{-6}) m/s. With the interface velocity of O(10^{-3}) m/s when production frequency is ~10 Hz, v_{eof} is slow enough to be ignored compared to interface velocity induced by electric stress.

(b) R_1, R_2, and R_3 for each channel

Table S2. Electrical resistances of the long microchannel (R_1), channel neck (R_2), liquid/liquid interface (R_3), and reservoirs (R_{res}) for four different channel designs.

L/D_H	R_1 [$M\Omega$]	R_2 [$M\Omega$]	R_3 [$M\Omega$]	R_{res} [$k\Omega$]
2.5	1.6	0.83	4.5	1.1
5.8	1.5	1.1	1.6	1.1
10	3.3	3.2	4.4	1.1
12.5	1.6	3.3	4.3	1.1

3. Calculation of emulsion sizes using *I–t* graph

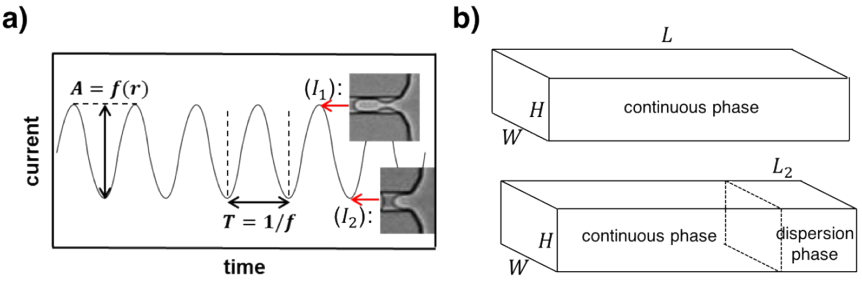

Figure S3. (a) Current–time (*I–t*) graph for the period when emulsions are generated inside the channel neck. (b) Upper image shows the case where the continuous phase completely fills the channel neck, corresponding to the lowest current value (I_2) in the *I–t* graph. The lower image shows the case where the dispersion phase completely fills the channel neck, corresponding to the highest current value (I_1) in the *I–t* graph.

Fig. S3(a) shows the continuous *I–t* graph for the case where discrete emulsions are produced by the electric field inside the channel neck. If the resistivity of the continuous phase (ρ_c) is greater than that of the dispersion phase (ρ_d), the current exhibits its maximum value (I_1) when the dispersion phase completely fills the channel neck. Therefore, this point is synchronized with the moment when the emulsions are detached from the interface. After the emulsion detachment, the interface is pulled back to its original position by the interfacial tension until the current exhibits its minimum value (I_2).

The electrical resistance of the channel neck, as it corresponds to the upper part of Fig. S3(b), or as it is fully filled with the continuous phase, is

$$R_a = \rho_c \frac{L}{WH} \tag{S5}$$

Next, when the emulsion is about to break up (lower part of Fig. S3(b)), the dispersion phase fills the channel neck with a volume of $W \times H \times L_2$. The electrical resistance of the channel at this moment is

$$R_b = \rho_c \frac{L - L_2}{WH} + \rho_d \frac{L_2}{WH}. \quad \text{(S6)}$$

If the radius of the fabricated emulsion is r, $W \times H \times L_2$ is equal to the fabricated emulsion volume; thus,

$$L_2 = \frac{\frac{4}{3}\pi r^3}{WH}. \quad \text{(S7)}$$

Then, Eq. (S5) can be rewritten as

$$R_b = \rho_c \left(\frac{L}{WH} - \frac{4\pi r^3}{3W^2H^2}\right) + \rho_d \frac{4\pi r^3}{3W^2H^2}. \quad \text{(S8)}$$

The amplitude of the current peak in Fig. S3(a) can be calculated using the electrical-resistance difference between I_1 and I_2, as indicated by the following expression, where V represents the applied external voltage:

$$A = \Delta I = V\left(\frac{1}{R_1 + R_b + R_3} - \frac{1}{R_1 + R_a + R_3}\right). \quad \text{(S9)}$$

Eq. (S9) can be rewritten as

$$A = V\left[\frac{4\pi r^3}{3W^2H^2}(\rho_c - \rho_d)\left(\frac{1}{(R_1 + R_a + R_3)(R_1 + R_b + R_3)}\right)\right]. \quad \text{(S10)}$$

If $\rho_c > \rho_d$, as is the case with the two-phase system used in this study, $R_a > R_b$, and if R_b is assumed to be negligible, the radius r can be expressed as

$$r \approx \sqrt[3]{\frac{A}{V} \times \frac{3W^2H^2}{4\pi(\rho_c - \rho_d)} \times (R_1 + R_3) \times \left(R_1 + R_3 + \rho_c \frac{L}{WH}\right)}. \quad \text{(S11)}$$

This assumption (R_b can be ignored when $R_a > R_b$) is valid because the r values calculated by ignoring R_b (Eq. (S11)) and without ignoring R_b (Eq. (S10)) exhibited little discrepancies. When computed using the Mathematica equation solver, the r values exhibited only ~7% error between Eqs. (S10) and (S11). Thus, if the applied voltage, V, and current-change amplitude , A, are known from experiments, the fabricated emulsion radii can be predicted using the foregoing equation. The average current-amplitude changes in the channel neck with an aspect ratio of 5.8 from 40–80 V are presented in Table S3.

According to Baroud et al.[3], when discrete emulsions or droplets of the dispersion phase fill the microchannel, there always exist lubrication films between the dispersion-phase emulsion and the microchannel, provided that the continuous phase has a higher affinity to the channel walls. In this context, it can be predicted that there will be lubrication films surrounding the emulsions moving inside the bottleneck channel of our system, because the continuous phase (PEG-phase) has a higher affinity with the PDMS channel wall and higher hydrophobicity compared with the dispersion phase (salt-phase). Because the liquid/liquid interface induces the discontinuity in the electric field[4], we can conclude that the current will preferentially flow through the lubrication films of the continuous phase around the detached emulsions. This was verified in Supplementary Material Section 2, by the high electrical resistance of the liquid/liquid interface. With the discontinuity in the electric field across the interface of the detached emulsions inside the bottleneck channel and the presence of lubrication films, almost no part of the electric field flowing inside the channel is consumed at the interfaces of already detached emulsions. This can be proven by the absence of acceleration or changes in the interface shapes of the emulsions moving inside the bottleneck channel via electrophoresis (Supplementary Video S1 and Fig. 2).

As reported by other groups[5-7], the electric field applied at the liquid/liquid interface exerts electrical stress, which deforms the interface shape in the direction of the electric field and generates flow fields inside and around the interface. Hence, in our system, the electrical stress is mainly applied at the liquid/liquid interface located at the end of the bottleneck channel, because it is continuously extruded toward the direction of the electric field until emulsification is achieved by the balance of the electrical stress and the interfacial tension stress. No other interfaces or emulsion surfaces exhibit deformations caused by the electrical stress. Therefore, we can safely neglect the existence of previously produced emulsions inside the bottleneck channel when theoretically calculating the current drop caused by the protrusion and retrusion of the dispersion phase inside the bottleneck channel.

Table S3. Average current peak amplitudes of the *I–t* graphs for different applied external voltages. The channel neck has an aspect ratio ($^{L}/_{D_H}$) of 5.8, which was used for the experiment.

	$40\ V$	$50\ V$	$60\ V$	$70\ V$	$80\ V$
$\Delta I\ [A]$	8.3×10^{-7}	7.1×10^{-7}	5.5×10^{-7}	4.6×10^{-7}	3.7×10^{-7}

4. Extended normalized *I–t* curve showing stable emulsification over 2 min in dripping regime

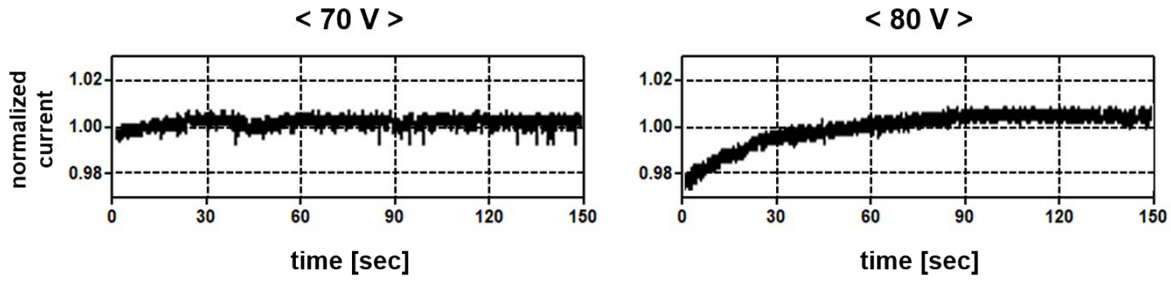

Figure S4. Stable emulsification in the dripping regime for the channel with the geometry shown in Fig. 2(b) of the main manuscript. Over 2 min of emulsification without a significant change in the current amplitude was achieved.

5. Extended phase diagram showing threshold condition and hysteresis of dripping regime

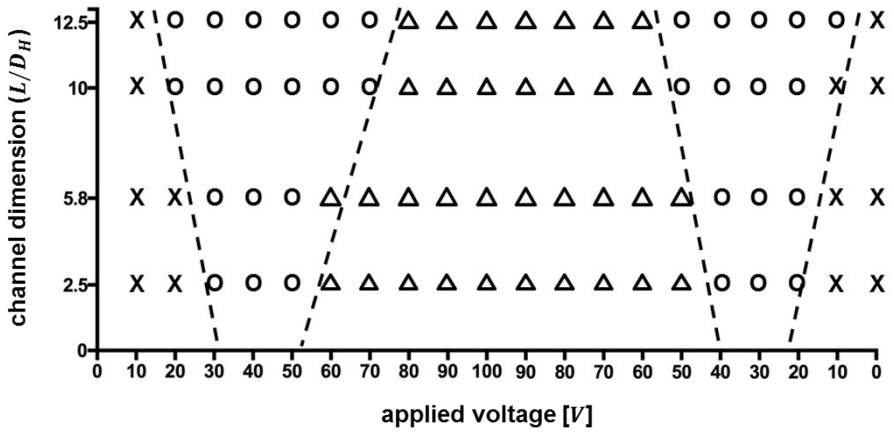

Figure S5. Extended phase diagram for emulsion generation. The applied voltage was increased from 0 to 100 V and then reduced to 0 V to evaluate the threshold electric-field strength hysteresis. The threshold electric-field strength decreased when the applied voltage decreased.

6. Polydispersity of fabricated emulsion radii dataset of microchannel having aspect ratio of 5.8

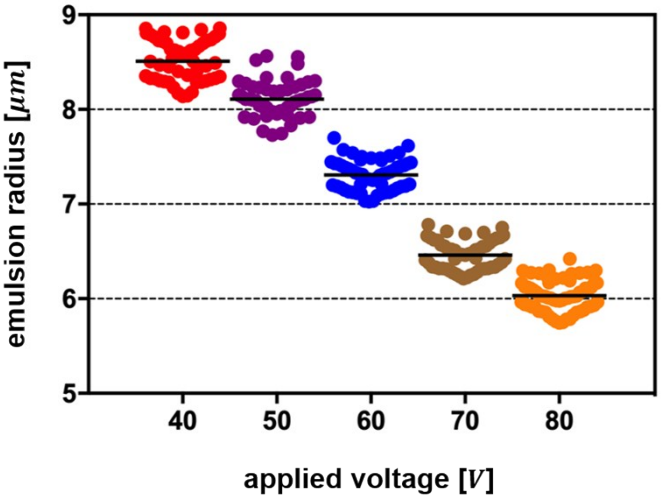

Figure S6. Plot showing the polydispersity of the fabricated emulsion radii distribution for a microchannel having a bottleneck geometry with an aspect ratio of 5.8. These are optically measured values.

References

1. Xuan, X.; Xu, B.; Sinton, D.; Li, D., Electroosmotic flow with Joule heating effects. *Lab on a Chip* **2004,** *4* (3), 230-236.
2. Forciniti, D.; Hall, C. K.; Kula, M. R., Interfacial tension of polyethyleneglycol-dextran-water systems: influence of temperature and polymer molecular weight. *Journal of Biotechnology* **1990,** *16* (3), 279-296.
3. Baroud, C. N.; Gallaire, F.; Dangla, R., Dynamics of microfluidic droplets. *Lab on a Chip* **2010,** *10* (16), 2032-2045.
4. Bentenitis, N.; Krause, S., Droplet Deformation in Dc Electric Fields: The Extended Leaky Dielectric Model. *Langmuir* **2005,** *21* (14), 6194-6209.
5. Lac, E.; Homsy, G. M., Axisymmetric deformation and stability of a viscous drop in a steady electric field. *Journal of Fluid Mechanics* **2007,** *590*, 239-264.
6. Lin, Y.; Skjetne, P.; Carlson, A., A phase field model for multiphase electro-hydrodynamic flow. *International Journal of Multiphase Flow* **2012,** *45*, 1-11.
7. Singh, R.; Bahga, S. S.; Gupta, A., Electrohydrodynamics in leaky dielectric fluids using lattice Boltzmann method. *European Journal of Mechanics - B/Fluids* **2019,** *74*, 167-179.